

Burn-In Demonstrations for Multi-Modal Imitation Learning

Alex Kuefler

Symbolic Systems Program
Stanford University
Stanford, CA 94305
akuefler@stanford.edu

Mykel J. Kochenderfer

Department of Aeronautics & Astronautics
Stanford University
Stanford, CA 94305
mykel@stanford.edu

Abstract

Recent work on imitation learning has generated policies that reproduce expert behavior from multi-modal data. However, past approaches have focused only on recreating a small number of distinct, expert maneuvers, or have relied on supervised learning techniques that produce unstable policies. This work extends InfoGAIL, an algorithm for multi-modal imitation learning, to reproduce behavior over an extended period of time. Our approach involves reformulating the typical imitation learning setting to include “burn-in demonstrations” upon which policies are conditioned at test time. We demonstrate that our approach outperforms standard InfoGAIL in maximizing the mutual information between predicted and unseen style labels in road scene simulations, and we show that our method leads to policies that imitate expert autonomous driving systems over long time horizons.

Introduction

Modeling human behavior is necessary for developing and validating autonomous systems. In the context of autonomous driving, modeling drivers is challenging because there is significant variability in driving style and behavior. Latent factors, such as a person’s degree of attentiveness or their willingness to take risks may influence the type of driving behavior they demonstrate. As a result, a distribution of expert demonstrations of some sequential decision making task may have multiple modes, resulting from factors that are difficult to measure.

One line of research attempts to discover latent factors underlying expert demonstrations using fully differentiable models trained with stochastic gradient variational Bayes (Kingma and Welling 2013; Watter et al. 2015). In robotics, variational autoencoders (VAE) have been used to discover latent embeddings of human demonstrations, allowing classical controllers to act in feature spaces that obey desirable properties (Watter et al. 2015). VAEs have also been used to learn shared embedding spaces for different *sensor* modalities, allowing a single model to reconstruct, for example, the motion of a stroke from an image of a handwritten digit (Yin et al. 2017). More recently, this model family has been applied to discover different *actuation* modalities, as in the case of demonstrations that share the same observation space, but were sampled from experts who obey different policies. In the context of autonomous driving, driver modeling is

treated as a conditional density estimation problem, where the model is trained by conditioning on driver observations and predicting actions (e.g., acceleration and turnrate) from the expert demonstrations alone. Such models can be fit without gathering new data in simulation, and can thus discover latent factors in expert demonstrations directly (Morton and Kochenderfer 2017). However, policies trained with supervised learning are sensitive to minor prediction errors, making this approach impractical for many sequential decision making problems (Ross and Bagnell 2010).

Alternatively, methods based on Generative Adversarial Imitation Learning (GAIL) combine supervised and reinforcement learning by conducting rollouts in a simulation environment (Ho and Ermon 2016). Human demonstrations and policy rollouts can then be compared by a critic, which is trained to provide high reward when the policy’s behavior becomes indistinguishable from those of experts. Information Maximizing GAIL (InfoGAIL), in particular, addresses the problem of learning policies from multi-modal demonstrations, and has been used to produce driver models that can give rise to different passing and turning behaviors (Li, Song, and Ermon 2017). However, InfoGAIL and related techniques (Hausman et al. 2017) involve sampling a latent code at the beginning of each trial. If the simulated ego-vehicle is initialized with the velocity and heading of a real driver, the random sampling of latent codes can not ensure consistency between the policy’s subsequent actions and the driver’s true style. This shortcoming limits the applicability of InfoGAIL to modeling real highway scenes, where ego vehicles are sampled from playbacks of recorded human data (Kuefler et al. 2017).

We introduce *Burn-InfoGAIL*, an imitation learning technique that addresses this limitation by drawing latent codes directly from a learned, inference distribution (Zhao, Song, and Ermon 2017). Like recent work on one-shot (Duan et al. 2017) and diverse imitation learning (Wang et al. 2017), our models not only learn from a set of demonstrations, but also condition upon specific reference demonstrations at the beginning of each rollout in a simulated environment. However, Burn-InfoGAIL assumes a new task formulation, motivated by simulated driving. In this setting, a policy must take over from the point at which a specific expert demonstration ends, such as when steering is engaged in an autonomous car. We refer to the partial, expert trajectory as a *burn-in* demon-

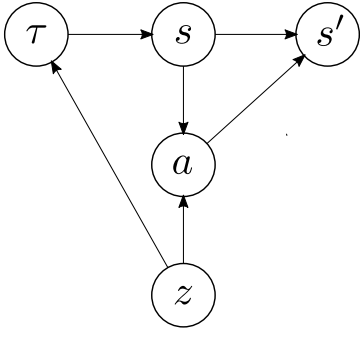


Figure 1: Dynamic Bayesian network model of driver style. A latent factor z determines the underlying style of driver behavior. Vehicles progress according to an expert rollout τ , which is a sequence of states and actions carried out by a human driver or hand-crafted controller. The learned policy is conditioned on this history to select an action a , which positions the model in a subsequent state s' as determined by the dynamics of the environment.

stration, upon which the learned inference model must be conditioned in order to draw latent codes. This work demonstrates that Burn-InfoGAIL is able to achieve greater adjusted mutual information (AMI) with true driver styles than standard InfoGAIL or a variational autoencoder (VAE) baseline. Furthermore, we show that driving trajectories produced by Burn-InfoGAIL deviate less from expert demonstrations than GAIL, InfoGAIL, or supervised learning techniques.

Problem Formulation

We adopt a dynamic Bayesian network model of driver style (Morton and Kochenderfer 2017). Each vehicle is characterized by a unique *style* variable z , which influences the action a_t taken in response to an observation s_t seen at time t . In this work, we assume a vehicle’s trajectory through this environment proceeds in two stages. First, actions are chosen according to an expert policy π_E obeying style z for a burn-in demonstration lasting T time steps beginning by first observing s_0 . Starting with s_{T+1} , actions are then sampled until early termination or time horizon H according to a learned policy π_θ , parameterized by θ . We will use $\tau = (s_0, a_0, \dots, s_T, a_T)$ to denote the sequence of observations and actions occurring during the burn-in demonstration. The generative process that gives rise to our data (shown in Figure 1) factorizes according to:

$$p(s, a, z, \tau) = p(z)p(\tau | z)p(s | \tau)p(a | s, z) \quad (1)$$

$$= p(\tau)p(s | \tau)p(z | \tau)p(a | s, z) \quad (2)$$

where $s = s_{T+1}$, and the factors $p(a | s, z)$ and $p(\tau)$ may be interpreted as π_θ and a distribution over expert trajectories respectively. The factor $p(s | \tau)$ corresponds to the transition dynamics of the environment, which leaves $p(z | \tau)$ to be estimated from data. In our setting, the actions a are two dimensional vectors encoding the acceleration and turn-rate of the ego-vehicle. The observation s consists of both

hand-selected and low-level features, described in the implementation section.

Approach

We propose a new variation to GAIL, which discovers latent factors in expert demonstrations while learning different driving policies. Unlike past work, we assume a setting in which our policy not only learns from demonstrations, but conditions on individual trajectories, continuing from where expert demonstrations stopped. This section describes the objectives we wish to optimize in order to discover both latent intentions and stable policies.

Imitation Learning

In the imitation learning setting, we wish to train a policy π_θ that captures behavior similar to those of an expert policy π_E . Because the reward optimized by π_E is unknown, GAIL (Ho and Ermon 2016) introduces a discriminator D_ω , parameterized by ω , that can help π_θ improve by distinguishing expert from non-expert actions. GAIL minimizes with respect to θ and maximizes with respect to ω the objective:

$$V(\theta, \omega) = \mathbb{E}_{a \sim \pi_E(\cdot | s)}[\log D_\omega(s, a)] + \mathbb{E}_{a \sim \pi_\theta(\cdot | s)}[\log(1 - D_\omega(s, a))] \quad (3)$$

Recent variants of GAIL (Li, Song, and Ermon 2017) replace the discriminator with a *critic*, which outputs a real-valued score rather than a probability. We adopt this formulation and train D_ω to minimize the Wasserstein objective,

$$W(\theta, \omega) = \mathbb{E}_{a \sim \pi_\theta(\cdot | s)}[D_\omega(s, a)] - \mathbb{E}_{a \sim \pi_E(\cdot | s)}[D_\omega(s, a)] \quad (4)$$

learning to output a high score when encountering pairs produced by π_E , and a low score when conditioned upon outputs from a policy. The output of the critic $D_\omega(s, a)$ can then be used as a surrogate reward function $\tilde{r}(s, a)$. Assuming an appropriate value for ω , the surrogate reward increases as actions sampled from π_θ look similar to those chosen by experts. In our setting, π_θ may end a training trial prematurely by causing a collision or going off-road. To discourage early stopping, we define $\tilde{r}(s, a)$ to be always positive,

$$\tilde{r}(s, a) = \log(1 + e^{D_\omega(s, a)}) \quad (5)$$

Optimizing equations 3 and 4 has lead to policies that reproduce expert performance in a number of settings (Ho and Ermon 2016; Li, Song, and Ermon 2017; Kuefler et al. 2017). However, the behavior of these policies tend to be unimodal, failing to account for different latent styles.

Information Maximization

In standard variational information maximization (Barber and Agakov 2003), the objective is to maximize the mutual information between a generator and posterior $p(z | s, a)$ over latent codes by optimizing a lower bound. In contrast, we view $q(z | s, a)$ as an inference distribution with associated marginal $q(z)$, rather than a variational approximation to $p(z | s, a)$ (Zhao, Song, and Ermon 2017). We propose maximizing the mutual information between our policy and the

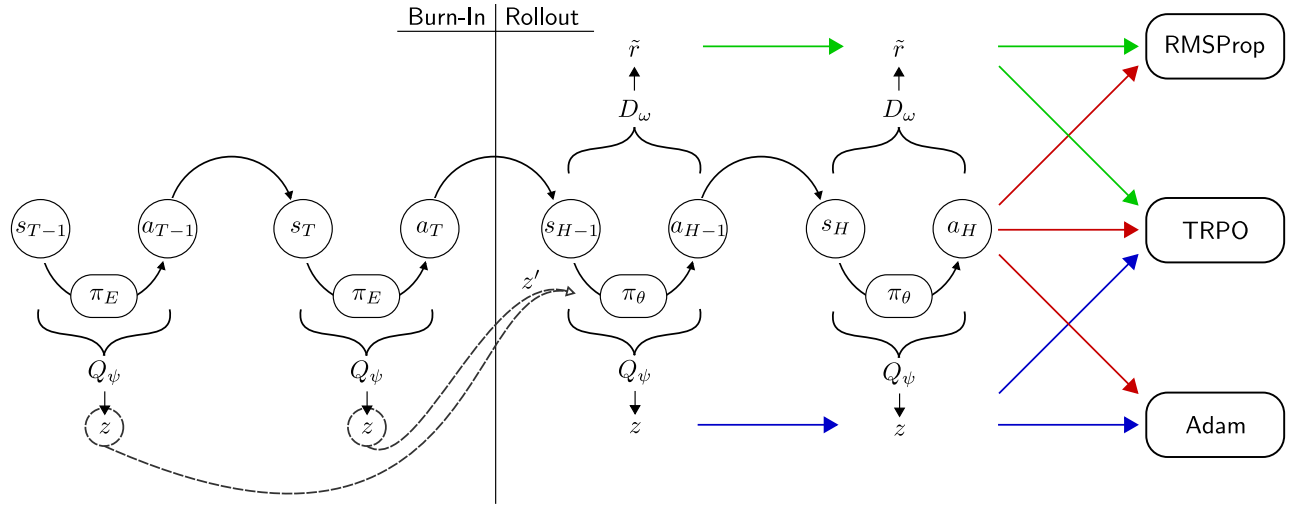


Figure 2: Diagram of Burn-InfoGAIL. The expert π_E selects actions during the burn-in demonstration, whereas learned π_θ selects actions during the rollout. Dashed lines represent the majority vote taken over predicted latent codes z to produce the initial z' for the rollout. Red arrows represent the contribution of the state-action pairs to the RMSProp, TRPO, and Adam optimizers. Blue arrows represent the contribution of z , and green arrows represent the contribution of critic outputs \tilde{r} .

joint inference distribution directly, using the factorization in equation 2:

$$I_q(z; s, a) = \mathbb{E}_{q(s, a, z, \tau)} [\log q(z | s, a) - \log q(z)] \quad (6)$$

$$= \mathbb{E}_{\tau, s, z', a} [\log q(z' | s, a)] - \mathbb{E}_{z'} [\log q(z')] \quad (7)$$

$$= H(Q_\psi(z')) - C(\theta, \psi) \quad (8)$$

where $\tau \sim p(\tau)$ is drawn randomly from a distribution of burn-in demonstrations, the initial observation for the rollout $s \sim p(s | \tau)$ is determined by the environment dynamics, and the target latent code $z' \sim q(\cdot | \tau)$ and initial action $a \sim \pi_\theta(\cdot | s, z')$ must be sampled from learned models.

The model Q_ψ is a parametric representation of the inference distribution $q(z | s, a)$, parameterized by ψ . The objective $C(\theta, \psi)$ is simply the cross entropy error between the latent code z' sampled at the beginning of the trial, and the code predicted by Q_ψ at the end, which is minimized in standard InfoGAIL. However, we now sample z' from the inference model $Q_\psi(z' | \tau)$ conditioned on the burn-in demonstration τ , rather than an arbitrary prior. The term $H(Q_\psi(z'))$ is analogous to the entropy over latent codes derived in past work (Chen et al. 2016; Hausman et al. 2017). Because we now sample codes from $Q_\psi(z | \tau)$ at the beginning of each trial, $Q_\psi(z') = \mathbb{E}_\tau[Q_\psi(z' | \tau)] \approx \hat{\mathbb{E}}_\tau[Q_\psi(z' | \tau)]$ must be approximated using Monte Carlo estimation.

Burn-InfoGAIL

Combining equations 4 and 8, the final form of our objective is given by:

$$\min_{\theta} \max_{\omega, \psi} \underbrace{W(\theta, \omega)}_{\text{Imitation}} - \underbrace{C(\theta, \psi)}_{\text{Style}} + \lambda \underbrace{H(\hat{\mathbb{E}}_\tau[Q_\psi(z' | \tau)])}_{\text{Entropy}} \quad (9)$$

where λ is a hyperparameter controlling the weight of the entropy. The first term encourages the model to imitate the

driver data, and the second term allows it to perform its imitation in such a way that the driver class can be predicted from its actions. The third term ensures that the inference model will, on average, sample from among all the latent codes.

Assuming that driver styles are distributed uniformly in the true data set, $H(Q_\psi(z'))$ can be interpreted as the Kullback-Leibler (KL) Divergence between the expected value of the inference model and prior distribution. In other words, we sample a code z by conditioning our model on the burn-in demonstration to ensure that the latent code reflects the actual style of the expert each trial. Because the optimization wants to minimize $C(\theta, \psi)$, the sampling posterior may attempt to push its probability mass to a single label, so as to be maximally discriminable. Therefore, $H(Q_\psi(z'))$ must be maximized to ensure that, on average, samples from the posterior $Q_\psi(z | \tau)$ are uniformly distributed. This result leaves open the opportunity to extend our approach to different distributions of expert data by changing the prior over z , but we defer this question to future work.

Implementation

In practice, Burn-InfoGAIL requires an environment simulator in which to generate rollouts and parametric, conditional density estimators to represent the policy, critic, and inference model. This section explains how these components were implemented for our experiments.

Environment

The simulator used to generate data and train models is based on an oval racetrack, shown in Figure 3. As in past work (Morton and Kochenderfer 2017), we populate our environment with vehicles simulated by the Intelligent Driver Model (Treiber, Hennecke, and Helbing 2000), where lane changes

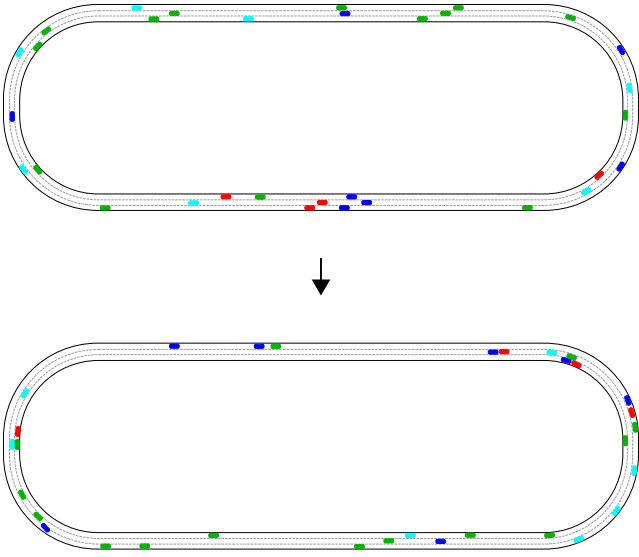


Figure 3: Scenes taken from oval track environment after initialization and a few seconds of driving. Over time, tail-gaiters (green) and aggressive drivers (red) cluster behind passive drivers (blue). Speeders (cyan) retain their large headway distances.

are executed by the MOBIL general lane changing model (Kesting, Treiber, and Helbing 2007). The settings of each controller are drawn from one of four possible parameterizations, defining the style z of each car. The resulting driving experts fall into one of four classes:

- *Aggressive*: High speed, large acceleration, small headway distances.
- *Passive*: Low speed, low acceleration, large headway distances.
- *Speeder*: High speed and acceleration, but large headway distance.
- *Tailgating*: Low speed and acceleration, but small headway distances.

Furthermore, the desired speed of each car is sampled from a Gaussian distribution, ensuring that individual cars belonging to the same class behave differently. A total of 960 training demonstrations and 480 validation demonstrations were used, each lasting 50 timesteps (or 5 seconds, at 10 Hz).

The observations are represented with a combination of LIDAR and road features (Kuefler et al. 2017; Morton and Kochenderfer 2017). We used 20 LIDAR beams, giving the policy access to both distance and range rate for surrounding cars. Road features included attributes such as the ego vehicle’s speed, lane offset, and distance to lane markings. We also include three indicator variables in the observation vector, which detect collision states, offroad events, and driving in reverse. We terminate training when any of these three indicators are activated. Between LIDAR distance, range rate, road features, and indicator variables, the complete observation vector amounts to a total of 51 attributes.

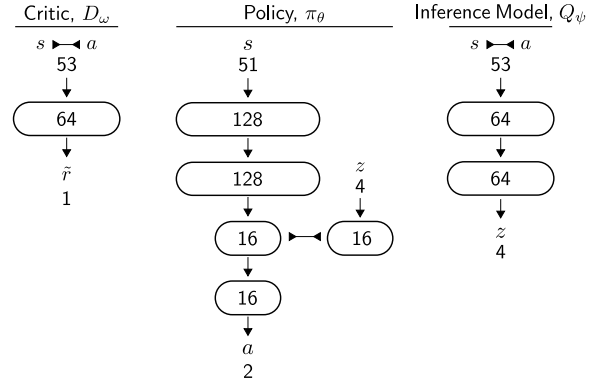


Figure 4: Network architecture for the policy π_θ , inference model Q_ψ , and critic D_ω . Directed arrows denote feedforward connections, bidirectional arrows denote concatenation, and integers denote the dimensionality of each layer.

Model Architecture

The models π_θ , D_ω , Q_ψ (shown in Figure 4) are represented by multilayer perceptrons (MLP) with \tanh activations. Actions are sampled $a \sim \mathcal{N}(\pi_\theta(\cdot | s, z), I\sigma)$ during training, where σ is also a trainable parameter vector. The 4-dimensional latent code z is passed into π_θ using a learned, linear embedding. Because the latent code is of a lower dimensionality than the input features, but we desire it to have a large influence on the outputs of π_θ , the embedding vector is concatenated with a later hidden layer of the policy network. The policy π_θ attempts to optimize the sum of discounted $\tilde{r}(s, a)$, which is not differentiable with respect to θ . However, policy gradient reinforcement learning can be used to approximate a gradient to train the model iteratively. In this work, we use Trust Region Policy Optimization (TRPO) (Schulman et al. 2015; Duan et al. 2016) to fit π_θ .

The inference model Q_ψ predicts the parameters of a categorical distribution. Note that although $Q_\psi(z | s, a)$ is a feedforward network, we condition on trajectories, predicting a value for each state-action pair and taking the most frequent prediction over the sequence. This network is simply trained to perform a 4-category classification task, where the “labels” for each example are generated at the beginning of the trial. Therefore, Q_ψ can be trained end-to-end with Adam, which leverages both momentum and feature scaling during stochastic gradient descent (Kingma and Ba 2014).

Finally, the objective used to update D_ω is also differentiable with respect to ω . The class labels (whether a state-action pair was produced by an expert, or π_θ) can be determined easily as well. However, Arjovsky, Chintala, and Bottou (2017) demonstrate that in order to obey the K-Lipschitz property, momentum free updates must be used to train the discriminator. Therefore, ω is fit using RMSProp (Tieleman and Hinton 2012).

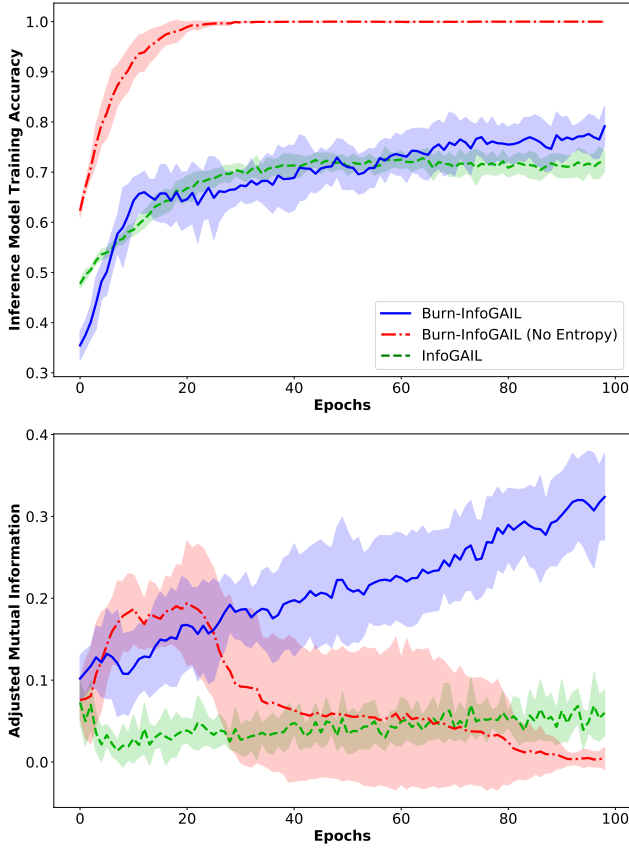


Figure 5: Training progress for both the reconstruction accuracy and adjusted mutual information obtained by the inference model, while varying the weight of entropy. Standard deviations were obtained by training 10 models for each experimental condition.

Experiments

In the following experiments, we evaluate π_θ as a model of driving behavior, and Q_ψ as an unsupervised, trajectory clustering technique. We would like to ensure that the values predicted by Q_ψ , when conditioned on expert trajectories, correlate with the underlying label z of the expert. As such, we use the adjusted mutual information (AMI) to measure performance (Vinh, Epps, and Bailey 2009).

Entropy and Mutual Information

We first experimented with different settings of λ in order to assess the role entropy maximization plays in our algorithm. Figure 5 shows that $\lambda = 0$ caused Q_ψ to converge to perfect classification accuracy with $\text{AMI}(Q_\psi(z | \tau), z) = 0$, as predicted. Figure 6 gives insight into this degenerate solution. We see that because Q_ψ produces its own labels at the beginning of the trial, it learns to collapse the entirety of its probability mass onto a single label (in this case, $Q_\psi(z | \tau) = 3$), so as to be maximally predictable. Conversely, when $\lambda = 500$, both AMI and classification accuracy increase over training epochs.

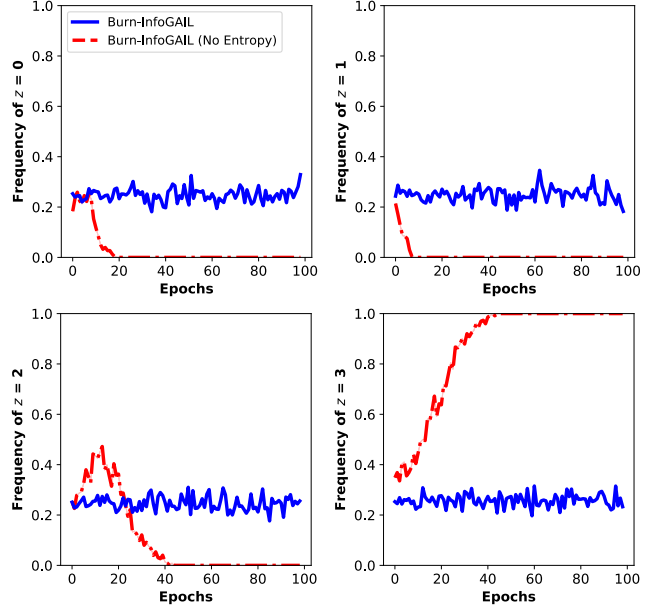


Figure 6: The frequency with which each latent code was sampled during model training with different λ . Entropy weighted models sample the classes uniformly throughout training, whereas models that do not use entropy converge to a single value.

After training, we applied the model achieving the highest AMI to a held out validation set of expert state-action pairs. Table 1 shows that the network outperforms other unsupervised learning techniques on unseen data, including the recurrent, variational autoencoder (VAE) first trained on this task environment (Morton and Kochenderfer 2017).

Reproducing Driving Behavior

Our next experiment tested how policies learned by Burn-InfoGAIL compared to other techniques for imitation learning. We randomly sampled 1,000 initial conditions and computed the root mean squared error (RMSE) of the speed and global position of learned policies versus expert driving behavior over 30 second trajectories. To ensure that all trajectories had consistent lengths for comparison, the vali-

Table 1: Adjusted mutual information scores of different models of $q(z | s, a)$ on validation set. Compares approaches that are unsupervised (U), supervised (S), and those that require a simulator to perform rollouts (R).

Method	Training	Validation AMI
K-Means	U	0.0
VAE + K-Means	U	0.24
InfoGAIL	U + R	0.16
Burn-InfoGAIL	U + R	0.38
SVM	S	0.95
VAE + SVM	S	0.22

Table 2: Frequency of dangerous events recorded over 1,000 rollouts, as a fraction of total timesteps.

Method	Offroad	Collision	Reversal
Burn-InfoGAIL	0.074	0.061	0.000
InfoGAIL	0.033	0.099	0.126
GAIL	0.165	0.059	0.177
VAE	0.756	0.021	0.000

dation environment did not end trials in the event of a collision, offroad, or reversal. Table 2 shows the frequency with which these “bad events” occurred during rollouts for each trial. Burn-InfoGAIL finds a good trade-off between going off-road and avoiding collisions, achieving a collision rate comparable to GAIL, but an off-road rate that is significantly smaller.

We compared against three baseline models: The first baseline is the VAE driver policy proposed by Morton and Kochenderfer (2017). Its encoder network consists of two Long Short-Term Memory (LSTM) (Hochreiter and Schmidhuber 1997) layers that map state-action pairs to the mean and standard deviation of a 2-dimensional Gaussian distribution. Its decoder, or policy, is a 2-layer MLP, also consisting of 128 units. During testing, the encoder conditions on the burn-in demonstration and the predicted mean of the distribution is used as the latent code for the policy. The second baseline is a GAIL model trained on the objective in equation 4. It has the same model architecture as π_θ , with the exclusion of the learned embedding layer needed to encode the style variable. Finally, we test against an implementation of InfoGAIL that is architecturally identical to π_θ , but simply samples z from a discrete uniform distribution at the beginning of each trial.

As shown in Figure 7, Burn-InfoGAIL achieves the lowest error over the longest period of driving. GAIL is able to capture differences in style for about 10 second, presumably because the imitation objective discourages the policy from adjusting its velocity away from its initial conditions. But as minor errors compound over long horizons, GAIL drifts towards an average policy due to its mode-seeking nature (Goodfellow 2016). In contrast, the VAE is able to use the latent code inferred from the burn-in demonstration to maintain an appropriate speed, achieving an RMSE close to the true value, rivaling Burn-InfoGAIL. However, being trained without a simulator, the VAE suffers from cascading errors causing it to go off road.

Qualitative Results

Observing that Burn-InfoGAIL obtains low RMSE over many trials, we produced visualizations to assess individual trajectories generated by each model. Figure 8a plots the global position of cars driven by each policy (including the IDM expert) over a 30 second period. We see that on the initial straightaway, all models perform comparably. However, the VAE baseline, trained with behavioral cloning, is unable to handle the turn. The GAIL-based techniques follow the curvature of the road more closely, but standard GAIL loses speed over time, ending its trial short of the expert’s position.

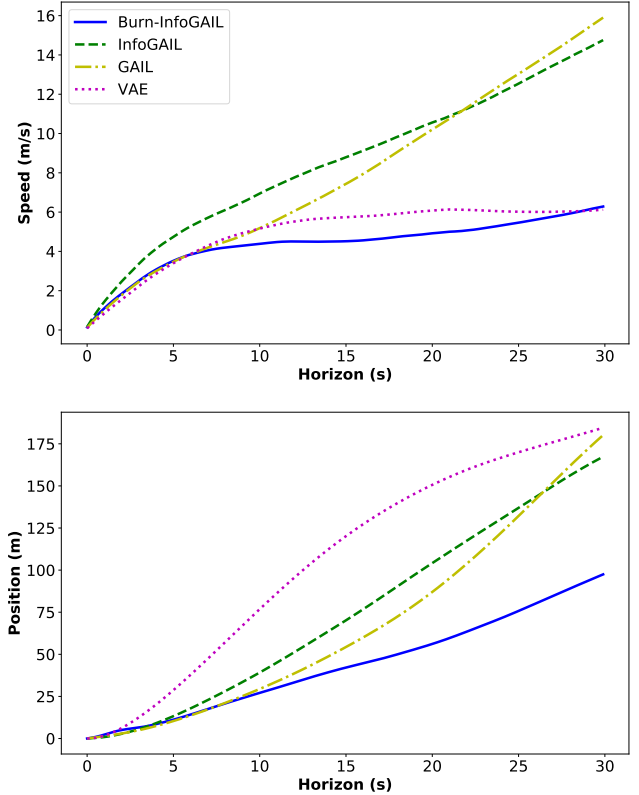


Figure 7: Root mean squared error (RMSE) between learned policies and validation trajectories. Results are averaged over 1,000 rollouts for each model. Our model achieves the lowest error on predicting both speed and position over 30 second trajectories.

Burn-InfoGAIL, in contrast, maintains the speed of the IDM throughout the drive, finding an endpoint that was closer to the ground truth than the other models.

Starting from the same road scene and ego vehicle, we next sought to understand how sampling different latent codes affected the policy’s behavior. Figure 8b plots the global position of the car obeying π_θ . Instead of conditioning our policy on a burn-in demonstration, we select z for 10 trials, for each possible code. We see that one code (red circle) seems to be designated for aggressive driving, changing lanes more regularly and driving farther (thus achieving a greater velocity) than the other trajectories. In contrast, another code appears to be designated for passive driving (blue star), performing fewer lane changes earlier on and ending closer to the starting position. Like the *speeder* and *tailgater* experts, the other codes tend to fall somewhere in between. When we visualize the learned embedding space of the latent codes by projecting its weight vectors onto two dimensions, we see a similar pattern emerge. Figure 9 demonstrates that most of the variance between the four embeddings is accounted for by the distance between the *aggressive* and *passive* codes, which have the greatest Euclidean distance from one another than the other codes.

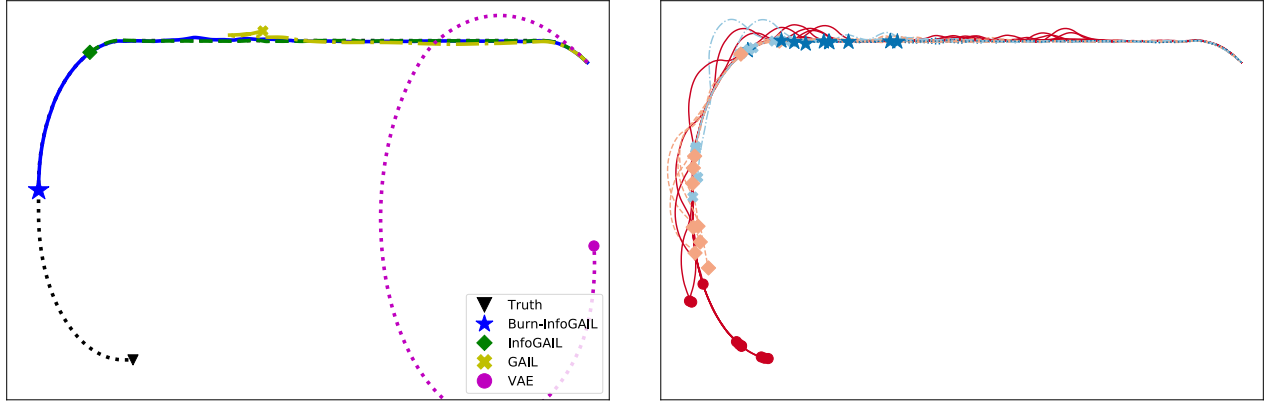


Figure 8: Model trajectories on track environment. Left: Example global positions of Burn-InfoGAIL along with baseline models and ground truth ego vehicle. Burn-InfoGAIL tends to end trials closer to the true end point. Right: Driving trajectories subject to sampling different latent codes. We see that terminal states tend to cluster on the basis of the latent code chosen.

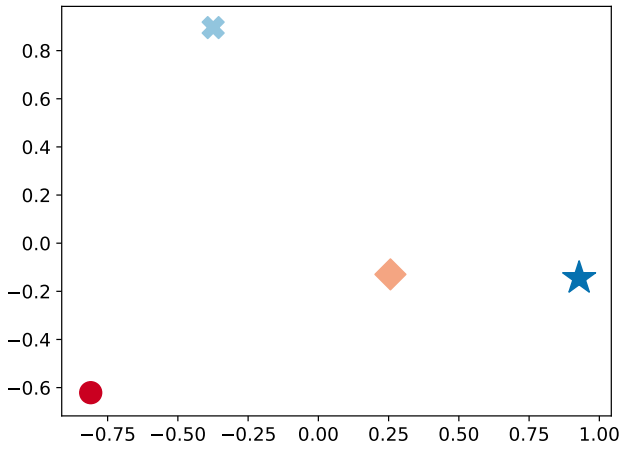


Figure 9: Learned embedding vectors (i.e., a subset of θ). Principal components analysis is used to express the 16 dimensional weight vectors in two dimensions. The difference between the most *passive* and *aggressive* driving codes accounts for most of the variance.

Conclusions

Humans perform many tasks expertly, albeit differently from one another. These differences between expert demonstrations are influenced by latent factors, or underlying styles, that may be determined long before demonstrations are recorded. InfoGAIL successfully extracts the latent factors controlling expert behavior for brief maneuvers (Li, Song, and Ermon 2017). Conversely, recurrent VAEs can identify long-term styles but rely on behavioral cloning, and thus produce unstable policies (Morton and Kochenderfer 2017). The contribution of this work has been to extend InfoGAIL to control and cluster expert trajectories governed by time invariant styles, as they may exist in sequential decision problems solved by humans. This work also introduced a new

formulation of the imitation learning paradigm in which initial states and latent factors are determined by a reference demonstration provided by an expert, and we showed that adopting this formulation along with the Burn-InfoGAIL algorithm leads to realistic models for a simulated, autonomous driving application.

In addressing this problem, we maximize mutual information with respect to a learned, inference distribution rather than maximizing a variational lower bound. We demonstrate that degenerate solutions may be avoided by maximizing the entropy in the estimated marginal distribution over latent codes. Our solution outperforms standard InfoGAIL in clustering time invariant driving styles, outperforming the state of the art on this task environment, while producing driver models that imitate experts over long horizons.

Burn-InfoGAIL appears to produce policies that use their learned, latent code to maintain their velocity over long time horizons. Whereas other GAIL-based approaches regress towards average behavior by the end of their trajectories, Burn-InfoGAIL terminates trials near the end-points of experts. Limitations of the model include its reliance on a simulated rollout environment, limiting its applicability as an unsupervised clustering method. Future work may explore ways to close the reinforcement learning loop, perhaps replacing the full simulation environment with a learned dynamics model for planning and learning from imagined rollouts.

We evaluated our approach on the assumption that expert styles are uniformly distributed, but Burn-InfoGAIL may extend to more uneven distributions. A promising research direction could involve replacing the entropy objective, here used to encourage diversity, with a general KL divergence term between the inference model and a more complex prior over latent codes. This approach may reveal connections between InfoGAIL and hierarchical reinforcement learning paradigms, where the inference distribution intelligently sets tasks as latent codes that the policy diligently follows.

Acknowledgments

We thank Jayesh Gupta, Jeremy Morton, Rui Shu, Tim Wheeler, and Blake Wulfe for useful discussions and feedback. This material is based upon work supported by the Ford Motor Company.

References

- Arjovsky, M.; Chintala, S.; and Bottou, L. 2017. Wasserstein GAN. *arXiv preprint arXiv:1701.07875*.
- Barber, D., and Agakov, F. 2003. The IM algorithm: A variational approach to information maximization. In *Advances in Neural Information Processing Systems (NIPS)*, 201–208.
- Chen, X.; Duan, Y.; Houthoof, R.; Schulman, J.; Sutskever, I.; and Abbeel, P. 2016. InfoGAN: Interpretable representation learning by information maximizing generative adversarial nets. In *Advances in Neural Information Processing Systems (NIPS)*, 2172–2180.
- Duan, Y.; Chen, X.; Houthoof, R.; Schulman, J.; and Abbeel, P. 2016. Benchmarking deep reinforcement learning for continuous control. In *International Conference on Machine Learning (ICML)*, 1329–1338.
- Duan, Y.; Andrychowicz, M.; Stadie, B.; Ho, J.; Schneider, J.; Sutskever, I.; Abbeel, P.; and Zaremba, W. 2017. One-shot imitation learning. *arXiv preprint arXiv:1703.07326*.
- Goodfellow, I. 2016. NIPS 2016 tutorial: Generative adversarial networks. *arXiv preprint arXiv:1701.00160*.
- Hausman, K.; Chebotar, Y.; Schaal, S.; Sukhatme, G.; and Lim, J. 2017. Multi-modal imitation learning from unstructured demonstrations using generative adversarial nets. *arXiv preprint arXiv:1705.10479*.
- Ho, J., and Ermon, S. 2016. Generative adversarial imitation learning. In *Advances in Neural Information Processing Systems (NIPS)*, 4565–4573.
- Hochreiter, S., and Schmidhuber, J. 1997. Long short-term memory. *Neural Computation* 9(8):1735–1780.
- Kesting, A.; Treiber, M.; and Helbing, D. 2007. General lane-changing model mobil for car-following models. *Transportation Research Record* (1999):86–94.
- Kingma, D., and Ba, J. 2014. Adam: A method for stochastic optimization. *arXiv preprint arXiv:1412.6980*.
- Kingma, D. P., and Welling, M. 2013. Auto-encoding variational bayes. *arXiv preprint arXiv:1312.6114*.
- Kuefler, A.; Morton, J.; Wheeler, T.; and Kochenderfer, M. 2017. Imitating driver behavior with generative adversarial networks. *arXiv preprint arXiv:1701.06699*.
- Li, Y.; Song, J.; and Ermon, S. 2017. Inferring the latent structure of human decision-making from raw visual inputs. *arXiv preprint arXiv:1703.08840*.
- Morton, J., and Kochenderfer, M. J. 2017. Simultaneous policy learning and latent state inference for imitating driver behavior. *arXiv preprint arXiv:1704.05566*.
- Ross, S., and Bagnell, D. 2010. Efficient reductions for imitation learning. In *International Conference on Artificial Intelligence and Statistics*, 661–668.
- Schulman, J.; Levine, S.; Abbeel, P.; Jordan, M.; and Moritz, P. 2015. Trust region policy optimization. In *International Conference on Machine Learning (ICML)*, 1889–1897.
- Tieleman, T., and Hinton, G. 2012. Lecture 6.5-rmsprop: Divide the gradient by a running average of its recent magnitude. *COURSERA: Neural networks for machine learning* 4(2).
- Treiber, M.; Hennecke, A.; and Helbing, D. 2000. Congested traffic states in empirical observations and microscopic simulations. *Physical Review E* 62(2):1805.
- Vinh, N. X.; Epps, J.; and Bailey, J. 2009. Information theoretic measures for clusterings comparison: is a correction for chance necessary? In *International Conference on Machine Learning (ICML)*, 1073–1080.
- Wang, Z.; Merel, J.; Reed, S.; Wayne, G.; de Freitas, N.; and Heess, N. 2017. Robust imitation of diverse behaviors. *arXiv preprint arXiv:1707.02747*.
- Watter, M.; Springenberg, J.; Boedecker, J.; and Riedmiller, M. 2015. Embed to control: A locally linear latent dynamics model for control from raw images. In *Advances in Neural Information Processing Systems (NIPS)*, 2746–2754.
- Yin, H.; Melo, F. S.; Billard, A.; and Paiva, A. 2017. Associate latent encodings in learning from demonstrations. In *AAAI Conference on Artificial Intelligence (AAAI)*, 3848–3854.
- Zhao, S.; Song, J.; and Ermon, S. 2017. Towards deeper understanding of variational autoencoding models. *arXiv preprint arXiv:1702.08658*.